CORA Cork Open Research Archive
Cartlann Taighde Oscailte Chorcaí

Title	High capacity binder-free nanocrystalline GeO2 inverse opal anodes for Li-ion batteries with long cycle life and stable cell voltage
Authors	McNulty, David;Geaney, Hugh;Buckley, Darragh;O'Dwyer, Colm
Publication date	2018-11-07
Original Citation	McNulty, D., Geaney, H., Buckley, D. and O'Dwyer, C. (2018) 'High capacity binder-free nanocrystalline GeO2 inverse opal anodes for Li-ion batteries with long cycle life and stable cell voltage', Nano Energy, 43, pp. 11-21. doi: 10.1016/j.nanoen.2017.11.007
Type of publication	Article (peer-reviewed)
Link to publisher's version	http://www.sciencedirect.com/science/article/pii/S2211285517306870 - 10.1016/j.nanoen.2017.11.007
Rights	© 2017 Elsevier Ltd. All rights reserved. This manuscript version is made available under the CC BY-NC-ND 4.0 license. - http://creativecommons.org/licenses/by-nc-nd/4.0/
Download date	2026-09-05 20:49:46
Item downloaded from	https://hdl.handle.net/10468/5478

UCC
University College Cork, Ireland
Coláiste na hOllscoile Corcaigh

Author's Accepted Manuscript

High Capacity Binder-free Nanocrystalline GeO_2 Inverse Opal Anodes for Li-ion Batteries with Long Cycle Life and Stable Cell Voltage

David McNulty, Hugh Geaney, Darragh Buckley, Colm O'Dwyer

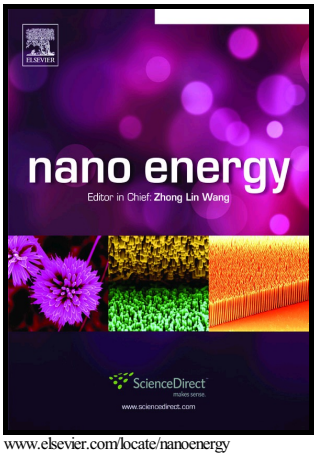

www.elsevier.com/locate/nanoenergy

PII: S2211-2855(17)30687-0
DOI: https://doi.org/10.1016/j.nanoen.2017.11.007
Reference: NANOEN2308

To appear in: *Nano Energy*

Received date: 23 July 2017
Revised date: 1 November 2017
Accepted date: 3 November 2017

Cite this article as: David McNulty, Hugh Geaney, Darragh Buckley and Colm O'Dwyer, High Capacity Binder-free Nanocrystalline GeO_2 Inverse Opal Anodes for Li-ion Batteries with Long Cycle Life and Stable Cell Voltage, *Nano Energy,* https://doi.org/10.1016/j.nanoen.2017.11.007

This is a PDF file of an unedited manuscript that has been accepted for publication. As a service to our customers we are providing this early version of the manuscript. The manuscript will undergo copyediting, typesetting, and review of the resulting galley proof before it is published in its final citable form. Please note that during the production process errors may be discovered which could affect the content, and all legal disclaimers that apply to the journal pertain.

ACCEPTED MANUSCRIPT

High Capacity Binder-free Nanocrystalline GeO_2 Inverse Opal Anodes for Li-ion Batteries with Long Cycle Life and Stable Cell Voltage

David McNulty[a], Hugh Geaney[a], Darragh Buckley[a] and Colm O'Dwyer[a,b*]

[a]*School of Chemistry, University College Cork, Cork T12 YN60, Ireland*

[b]*Micro-Nano Systems Centre, Tyndall National Institute, Lee Maltings, Cork T12 R5CP, Ireland*

Keywords: GeO_2, Inverse Opal, Li-ion, Semiconductor, Nanomaterials

Corresponding Author: *E-mail: c.odwyer@ucc.ie, Tel: +353 21 490 2732.

Accepted manuscript

Abstract

We demonstrate that crystalline macroporous GeO_2 inverse opals exhibit state-of-the-art capacity retention, voltage stability and a very long cycle life when tested as anode materials for Li-ion batteries. The specific capacities and capacity retention obtained from GeO_2 IOs are greater than values reported for other GeO_2 nanostructures and comparable to pure Ge nanostructures. Unlike pure Ge nanostructures, GeO_2 IOs can be prepared in air without complex processing procedures, potentially making them far more attractive from an industrial point of view, in terms of cost and ease of production. Inverse opals are structurally and electrically interconnected, and remove the need for additives and binders. GeO_2 IOs show gradual capacity fading over 250 and 1000 cycles, when cycled at specific currents of 150 and 300 mA/g, respectively, while maintaining high capacities and a stable overall cell voltage. The specific capacities after the 500^{th} and 1000^{th} cycles at a specific current of 300 mA/g were ~ 632 and 521 mAh/g respectively, corresponding to a capacity retention in each case of ~ 76% and 63% from the 2^{nd} cycle. Systematic analysis of differential capacity plots

ACCEPTED MANUSCRIPT

obtained from galvanostatic voltage profiles over 1000 cycles offers a detailed insight into the mechanism of charge storage in GeO_2 anodes over their long cycle life. Rate capability testing and asymmetric galvanostatic testing demonstrate the ability of GeO_2 IO samples to deliver significantly high capacities even at high specific currents (1 A/g).

Introduction

Recent advancements in portable consumer electronics have underscored the challenges facing next generation Li ion batteries. The identification of scalable, cost effective electrode materials which offer improved electrochemical performance compared to standard $LiCoO_2$/graphite cells is paramount to facilitate the production of future consumer-ready batteries.[1-4] Consequently, there has been a great deal of research focusing on the development of nanostructured anode and cathode materials for Li-ion and post Li-ion technologies. [5-9] On the anode side, alloying materials such as Si and Sn have been the subject of a tremendous amount of research with many mixed oxides of Sb and Sn demonstrating impressive cycling performance. [10-15] Germanium based anode materials have also attracted a lot of attention due to the high theoretical capacity of Ge (1384 mAh/g) with various nanostructures such as nanowires and nanoparticles being investigated as anode materials. [16-22] However the cost of preparing pure Ge nanostructures can be quite high due to the use of expensive anhydrous precursors such as diphenylgermane and the need to perform synthesis under an inert atmosphere. Low temperature routes to electrodeposited Ge microwires for battery anodes have been recently demonstrated using liquid Ga seed sources in water electrolytes, and show some promise.[23] High temperatures and costly precursors could also impede scaling up the synthesis of these materials for industrial applications. To circumvent these issues, we are investigating the electrochemical performance of GeO_2 with a structured macroporous morphology in the form of an inverse opal (IO), which can be

Accepted manuscript

ACCEPTED MANUSCRIPT

prepared in air using more cost-effective precursors. Previous reports on the electrochemical performance of GeO_2 as an anode material have indicated that the capacity values obtained from the oxide are lower than those obtained from pure Ge. [24-26] However, we demonstrate that by preparing a highly ordered, porous, three-dimensionally interconnected network of GeO_2 in the form of an IO, we can obtain capacity values which match the state of the art from pure Ge nanostructures grown from more complex, high temperature precursors.

In recent years, three-dimensional ordered macroporous (3DOM) materials such as IOs have proven very useful for increasing cycling stability and capacity retention. [27-33] The inherent physical properties of IO structured materials have many benefits for use as Li-ion battery electrode materials. The highly porous nature of IO structured materials allows a high surface area of the active material to be in direct contact with the electrolyte. [34, 35] The thin walls of the IO provide reduced Li ion diffusion path lengths compared to larger scale variants of the same material. Furthermore, the 3D networked nature of an IO structure can provide continuous transport paths and ensure good electronic and ionic conductivity and its interconnected structure has been proven to mitigate material disconnection and breakup that affects cycle longevity and capacity fade - polymeric binders are not required. [36]

Many commonly used Li ion battery materials possess low electronic conductivity. [37] The most prevalent method to overcome this issue is to prepare a composite consisting of the material under investigation with conductive carbon-based additives to increase the electrical conductivity. However, in practice the preparation of an interconnected conductive network is difficult to construct due to the tendency for small diameter carbon particles to aggregate, leading to non-homogeneous composites and since long life and safe Li batteries benefit from new materials development, [38, 39] methods for simple composition, long life anodes with stable voltages that compete with pure Li metal, remains an important goal. [40, 41] The inherent physical properties of an IO structure, discussed above can negate the need

Accepted manuscript

ACCEPTED MANUSCRIPT

for the preparation of conductive composites. For commercial applications, it is essential to develop simple, fast and low cost synthesis methods for electrode materials. Engineering battery materials into structures which do not need an additional step prior to electrochemical testing will reduce cost and ease industrial scale up. Stable material networks that maintain performance enhancing porous structure while limiting the reduction in tap density are important, and avoiding the need for 3D structured metallic current collectors improves gravimetric energy density. [42] We have previously shown that the electrochemical performance of V_2O_5, as a cathode material, can be significantly improved by engineering of nanoscale grains of V_2O_5 into an IO architecture. [43] Likewise we previously demonstrated the enhanced electrochemical performance of IO structured electrode materials with a full Li-ion cell consisting of a Co_3O_4 IO anode and a V_2O_5 IO cathode, and long life (>5000 cycles) stable cycling using rutile TiO_2 anodes in IO form. [44, 45]

In this report, we outline the nature of Ge nanocrystal-containing GeO_2 inverse opal Li-ion battery anodes that provide state of the art capacity, voltage stability and variable rate cycle life in a binder and conductive additive-free interconnected structure. The electrochemical performance of the GeO_2 IOs is evaluated via cyclic voltammetry, rate capability testing and long cycle life galvanostatic tests. GeO_2 IOs demonstrate stable, high capacity retention over 250 and 1000 cycles, at specific currents of 150 and 300 mA/g, respectively. Through systematic analysis of differential capacity plots (DCPs) from standard galvanostatic cycling as well as asymmetric cycling, we present a detailed insight into how GeO_2 anodes store charge and retain capacity with stable charge voltage during a long cycle life. Rate capability testing demonstates that the GeO_2 IOs are capable of delivering large reversible capacities with considerable capacity retention. Notably, the performance of the GeO_2 IOs was achieved in the absence of any binders or conductive additives. The ability to prepare a Ge-based anode material in air with cost effective precursors, without the need for

Accepted manuscript

ACCEPTED MANUSCRIPT

an inert atmosphere or any additional processing steps, such as the preparation of a slurry, which is capable of delivering stable, high capacity values and retention comparable to costly pure Ge nanostructures is a significant finding for high capacity Li-ion battery anodes.

Experimental Section

Preparation of GeO_2 IO

GeO_2 IO samples were prepared *via* infilling of a sacrificial polystyrene (PS) sphere template. The templates were prepared by drop casting a solution of PS spheres (Polysciences Inc., diameter = 500 nm) in isopropanol (IPA) on to 1 cm^2 pieces of stainless steel; the sphere templates were then infilled with a 0.05 M solution of germanium ethoxide ($Ge(OC_2H_5)_4$) in IPA. The infilled sphere templates were heated at 450 ^oC in air for 1 h, to remove the templates and to crystallize the samples.

Material Characterization

TEM analysis was conducted using a JEOL JEM-2100 TEM operating at 200 kV. SEM analysis was performed using an FEI Quanta 650 FEG high resolution SEM at an accelerating voltage of 10 kV. XRD analysis was performed using a Phillips Xpert PW3719 diffractometer using Cu Kα radiation. (Cu Kα, λ = 0.15418 nm, operation voltage 40 kV, current 40 mA). Raman scattering spectroscopy was performed using an Ocean Optics QE65PRO Raman Spectrometer with a Laser Quantum GEM DPSS single transverse mode CW laser emitting at λ = 532 nm and spectra were collected using a CCD camera. The beam was focused onto the samples using a 40× objective lens. XPS spectra were acquired on an Oxford Applied Research Escabase XPS system equipped with a CLASS VM 100 mm mean radius hemispherical electron energy analyzer with multichannel detectors in an analysis chamber with a base pressure of 5.0×10^{-10} mbar. Survey scans were recorded between 0 and

Accepted manuscript

ACCEPTED MANUSCRIPT

1400 eV with a step size of 0.7 eV, dwell time of 0.5 s, and pass energy of 100 eV. Core level scans were acquired with a step size of 0.1 eV, dwell time of 0.5 s, and pass energy of 20 eV averaged over 10 scans. A non-monochromated Al Kα X-ray source at 200 W power was used for all scans. All spectra were acquired at a take-off angle of 90° with respect to the analyzer axis and were charge corrected with respect to the C 1s photoelectric line. Data was processed using CasaXPS software where a Shirley background correction was employed and peaks were fitted to Voigt profiles. Photoluminescence (PL) spectroscopy was used to probe the electronic structure of the GeO_2 IOs. Investigation of the samples photoemission was carried out at room temperature using a 325 nm He–Cd laser excitation source with power density of 2 W/cm^2. PL spectra were recorded using a Horiba iHR320 spectrometer equipped with a thermoelectrically cooled Synapse CCD matrix.

Electrochemical Characterization

All electrochemical results presented in this report were performed using a BioLogic VSP Potentiostat/Galvanostat. The electrochemical properties of GeO_2 IO samples were investigated in a half cell configuration against a pure Li counter electrode in a two electrode, stainless steel split cell (a coin cell assembly that can be disassembled for post-mortem analysis). The electrolyte used consisted of a 1 mol dm^{-3} solution of lithium hexafluorophosphate salt in a 1:1 (v/v) mixture of ethylene carbonate in dimethyl carbonate with 3 wt% vinylene carbonate. The separator used in all split cell tests was a glass fiber separator (El-Cell ECC1-01-0012-A/L, 18 mm diameter, 0.65 mm thickness). The mass loading for all GeO_2 IO samples was ~ 0.5 – 1.0 mg, no additional conductive additives or binders were added. A Mettler Toledo XS205 Dualrange mass balance was used to determine the mass of IO material on the stainless steel substrates. The fine range tolerance of the mass balance is ± 0.01 mg and consequently the typical tolerance of our reported capacity values is ± 15 mAh/g. Cyclic voltammetry was performed using a scan rate of 0.1 mV s^{-1} in a potential

Accepted manuscript

ACCEPTED MANUSCRIPT

window of 1.5 – 0.01 V (vs Li/Li^+). Galvanostatic cycling was performed using a range of specific currents (250 – 1000 mA/g) in a potential window of 1.5 – 0.01 V (vs Li/Li^+). During the discussion of the electrochemical results, the lithiation process for our GeO_2 IO anode samples is referred to as the charging process and the delithiation process is referred to as the discharging process.

Results and discussion

GeO_2 IO samples were prepared via infilling of a PS sphere template, prepared on stainless steel, with a germanium (IV) ethoxide ($Ge(OC_2H_5)_4$) precursor solution. Thermal treatment of the infilled templates resulted in the decomposition of the sacrificial PS sphere template and the formation of a highly porous, crystalline, interconnected IO network as shown in the SEM and TEM images shown in Figure 1. Large regions of IO material are formed as shown in Figure 1a and the pore size for the GeO_2 IOs is typically ~ 450 nm as shown in Figure 1b. The cross-sectional thickness of a typical GeO_2 IO is ~ 13.4 μm, as shown in the tilt-corrected SEM image in Figure 1c. The thin walls of the GeO_2 IO, measured to be ~72 nm thick, the large surface area and the high level of porosity provide continuous transport paths for Li ions through the active phase (walls) and the electrolyte phase (pores). The high level of porosity and inherent interconnected structure of the 3D IO network is further demonstrated in the TEM image in Figure 1d. Similar to our previous work on transition metal oxide IOs prepared from chlorides, [43, 45, 46] the walls of GeO_2 IOs consist of an agglomeration of nanoparticles (NPs). Additional TEM images of the GeO_2 NP sub-structure of the IO walls are shown in Figure S1. The average diameter of the NPs which make up the walls of the GeO_2 IOs is ~25 nm, as shown in the histogram in Figure S1e. The electron

Accepted manuscript

diffraction (ED) pattern for a typical GeO_2 IO shown in Figure 1f, suggests a polycrystalline structure of pure hexagonal phase GeO_2.

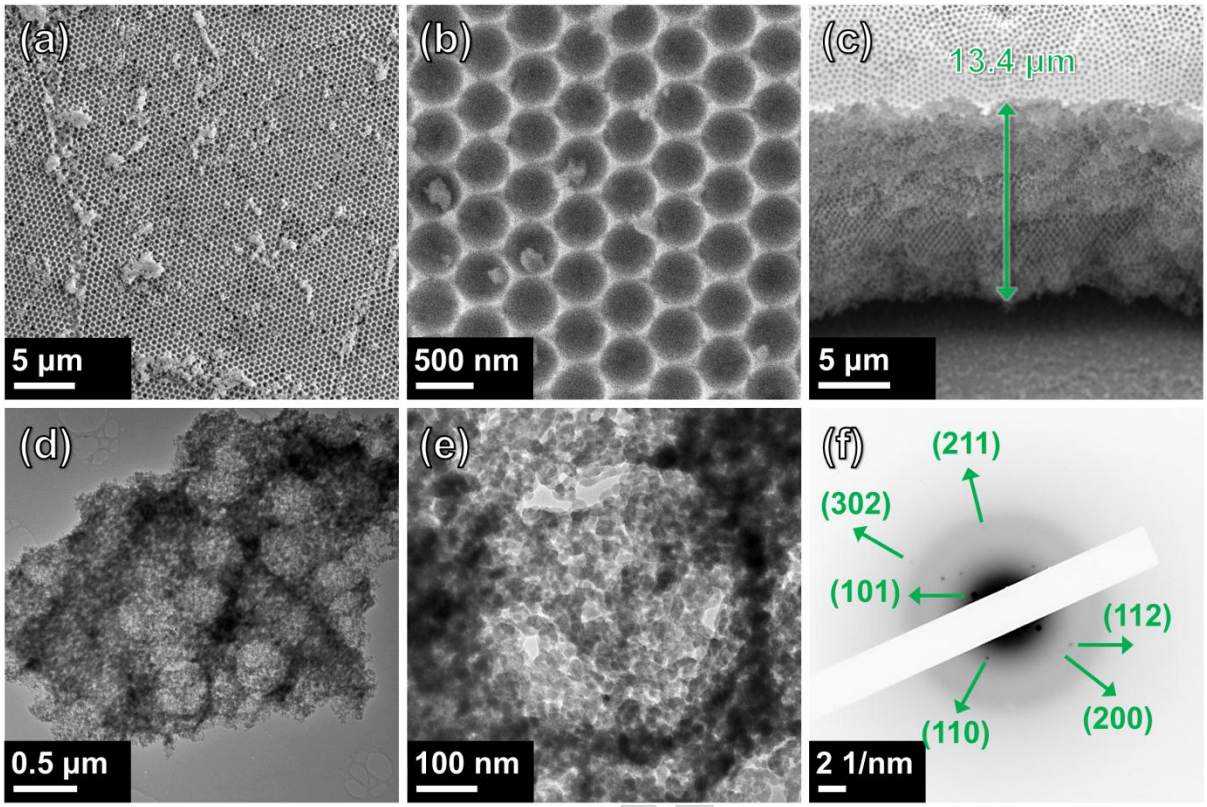

Figure 1. SEM images of showing (a) and (b) a top down view and (c) the cross-sectional thickness of a typical GeO_2 IO. TEM images of a typical GeO_2 IO showing (c) the porous structure and (d) the nanoparticles which comprise the walls of the IO. (f) Electron diffraction pattern of a typical GeO_2 IO.

The XRD pattern for a GeO_2 IO sample prepared on a stainless steel substrate is shown in Figure 2a. The reflections can be readily indexed to pure hexagonal GeO_2 (JCPDS No. 00-036-1463) with a *P3221* space group. From analysis of the XRD pattern, the calculated lattice parameters for our GeO_2 IO are a ~ 5.01 Å and c ~ 5.61 Å, giving a cell volume of ~ 121.95 $Å^3$. The Raman spectrum in Figure 2b for an as-prepared GeO_2 IO shows six Raman-active fundamental modes. The highest intensity peak at 419 cm^{-1}, as well the peaks at 234 and 253 cm^{-1} correspond to the A_1 mode of hexagonal GeO_2. [47] The peak present at 509 cm^{-1} corresponds to a characteristic mode of E symmetry split into a transverse

ACCEPTED MANUSCRIPT

optical (TO) mode for hexagonal GeO_2. [48] These phonon modes from GeO_2 IO are in excellent agreement with previous reports for hexagonal GeO_2,[49, 50] and are in agreement with our crystallographic analysis from XRD and electron diffraction. The two modes present at 305 and 575 cm^{-1} correspond to the first and second-order transverse optical (TO) phonon mode of crystalline Ge, indicating that there is some metalloid Ge present throughout the IO. [49, 51] An EDS spectrum for a GeO_2 IO was acquired over the area shown in the SEM image in the inset of Figure 2c. The spectrum confirms the presence of Ge, O and C within the IO structure. The characteristic C peak at ~ 0.27 keV is present due to the thermal decomposition of the germanium ethoxide ($Ge(OC_2H_5)_4$) precursor solution and the PS sphere template, as well as adventitious carbon on the surface of the IO. The atomic percentages (at.%) of each element present are listed in Table S1. From analysis of the at.%, the ratio of Ge:O is ~1:2, indicating a predominance of stoichiometric GeO_2 and some Ge phase throughout the IO volume.

To explore the chemical state of the crystalline Ge phases, an XPS spectrum of a GeO_2 IO sample displaying the Ge 3d core-level photoemission is shown in Figure 2d. Three main peaks can be seen at ~ 33.2, 34.6 and 36.2 eV, corresponding to the presence of Ge, GeO and GeO_2, respectively. [52] Comparison of the integrated peak areas associated with each Ge valence state indicates that the majority (~77.3%) of the Ge on the surface is present as Ge, ~14.9% is present in the GeO phase and ~7.8% is as GeO_2. As discussed, XRD analysis suggests that the IO samples are pure GeO_2 whereas Raman analysis indicates the IOs are GeO_2 with a presence of metalloid Ge. XPS analysis is in close agreement with observations from the Raman spectrum and suggests that the IOs may have a core-shell like electronic structure with the Ge present in the outer shell having a different oxidation state than in the inner core.

Accepted manuscript

ACCEPTED MANUSCRIPT

A photoluminescence (PL) spectrum was acquired to further investigate the presence of metalloid semiconducting crystalline Ge within the IO material, as shown in Figure 2e. Radiative band-to-band PL emission from indirect bandgap semiconductors such as Ge is possible in the quantum confinement (QC) regime [53], if the nanocrystal dimensions are below the exciton Bohr radius of ~24 nm for Ge. This value is very close to the average particle diameter measurements for the agglomerated nanocrystal-containing walls of the GeO_2 IOs. The PL emission consists of three peaks observed at ~490, 567 and 643 nm, corresponding to blue, green and orange emission, respectively. The broad PL peak with a band width from 510 to 710 nm was deconvoluted to demonstrate the relative intensity contributions from green and orange emissions, in Figure S2. A comparable blue emission at ~470 nm was observed in the PL spectrum for butyl-terminated Ge nanoparticles with an average diameter of 6.2 nm[54], however recent measurements reaffirm the doubt surrounding size-dependent bandgap values for nanocrystalline Ge in the blue region, and this emission most probably results from matrix effects, notably defects within the GeO_x. [55] Our measurements suggest that Ge nanocrystalline regions of dimensions less than 24 nm are also present throughout the IO material, and agrees with phonon mode analysis of crystalline Ge from Raman scattering spectra, but with a quantity too low to be detectable by XRD among crystalline GeO_2. A similar green emission has previously been reported for pure GeO_2 hollow walnuts and from a range of other complex, defective GeO_2 nanoparticle systems, thus confirming the presence of GeO_2, as seen from XRD and Raman analysis. [56] The orange band has previously been reported to originate from substoichiometric germanium oxides (GeO_x*s*), like many transition metal oxides, due to O vacancies.[57] Observations from the PL spectrum indicate that the IOs consist of nanoscale Ge–Ge bonded material (elemental Ge) and Ge–O bonded material, and this composition has implications for alloying reactions with Li.

Accepted manuscript

ACCEPTED MANUSCRIPT

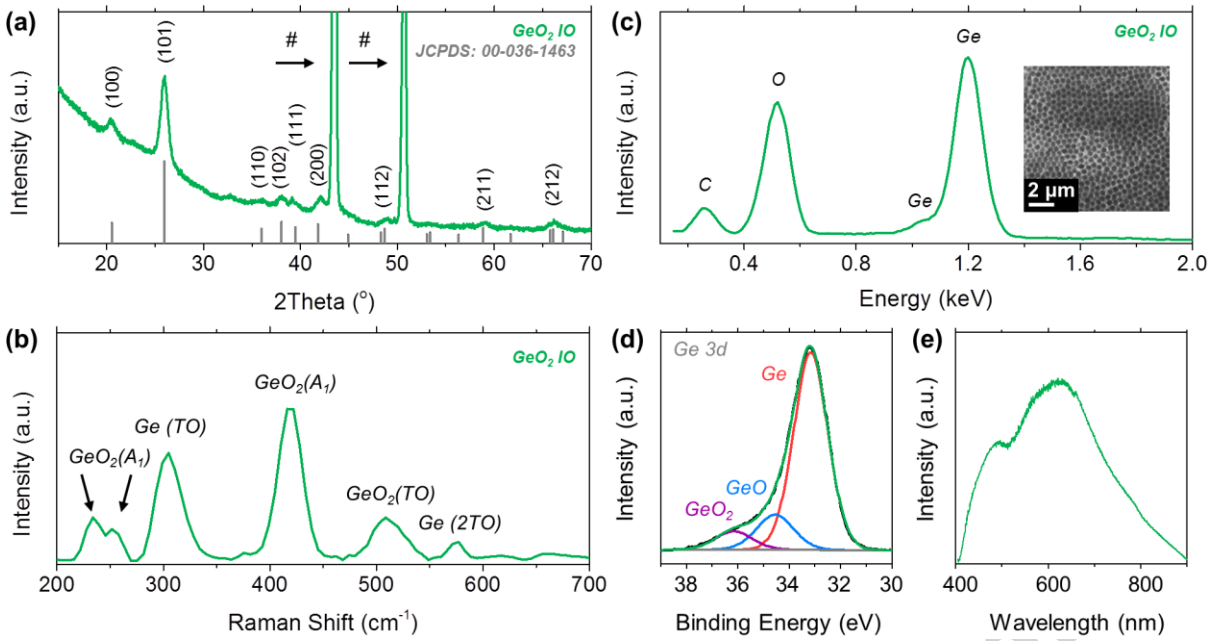

Figure 2. (a) XRD pattern for a GeO_2 IO prepared on a stainless steel substrate (reflections labelled # are stainless steel peaks). (b) Raman spectrum for a GeO_2 IO sample. (c) EDS spectra for a GeO_2 IO acquired from the area represented in the SEM image in the inset. (d) XPS spectra of the Ge 3d region for a GeO_2 IO. (e) Photoluminescence spectrum of a GeO_2 IO.

Cyclic voltammograms were acquired to investigate the Li^+ reaction mechanism for the GeO_2 IOs. The 1st, 2nd, 5th and 10th CV scans acquired at a scan rate of 0.1 mV/s are shown in Figure 3a. The broad peak centred at 1.15 V in the first cathodic sweep, which migrates to ~0.96 V from the second cycle onwards, (as shown in Figure S3a) can be attributed to the formation of amorphous Li_xGeO_2. [58, 59] The distinct peak at 0.78 V is likely due to the formation of the SEI layer as a peak at this potential is not observed in subsequent cycles. A peak attributed to the formation of the SEI layer at 0.75 V was reported for GeO_2 nanocrystals. [60] The cathodic peak at 0.45 V can be attributed to the reduction of Li_xGeO_2 and remaining GeO_2 into Ge and Li_2O. The sloping region in the first cathodic scan from ~ 0.3 to 0.01 V corresponds to the lithiation of crystalline Ge. [61] This may suggest that crystalline Ge is formed during the first cathodic scan via the electrochemical reduction of GeO_2 and from the second cycle onwards, the IO material is cycled as amorphous Ge. The

Accepted manuscript

ACCEPTED MANUSCRIPT

irreversible reduction of GeO_2 to Ge and subsequent cycling via alloying with Li has previously been reported for other GeO_2 nanostructures. Through in-situ XRD analysis Yoon et al. demonstrated that upon Li insertion (charging), the hexagonal phase of GeO_2 completely disappeared and after discharging the hexagonal phase did not reappear. [62] This will be discussed in greater detail through analysis of voltage-dependent differential capacity plots (DCPs) determined from galvanostatic cycling. From the second cycle onwards the sloping region begins at the higher potential of ~0.40 V, which is consistent with the lithiation of the a-$Li_{15}Ge_4$ (~0.35 V) and c-$Li_{15}Ge_4$ phases (~0.15 V). [63] The large broad asymmetric peak in the first anodic scan at ~ 0.50 V can be deconvoluted into two distinct peaks centred at 0.43 and 0.51 V, as shown in Figure S3b. These two peaks correspond to the delithiation of c-$Li_{15}Ge_4$ and a-$Li_{15}Ge_4$ phases respectively. [64] The broad asymmetric peak is shifted to the higher potential of ~0.55 V for the 5^{th} and 10^{th} cycles.

The electrochemical performance of GeO_2 IOs was also investigated via galvanostatic testing. A series of charge and discharge curves are shown in Figure 3b and c for a GeO_2 IO cycled 250 times using a specific current of 150 mA/g. The voltage profiles for the 1^{st} charge and discharge are shown in Figure 3b. The initial charge and discharge capacities were 2939 and 695 mAh/g, respectively, corresponding to an initial Coulombic efficiency (ICE) of ~ 24%. The large initial charge capacity can be attributed to the formation of an SEI layer on the surface of the IO as well as the formation of quasi reversible Li_2O. [65] A previous study on transition metal oxides suggested that thermal treatment under O_2/H_2O can introduce defects, such as cation vacancies, which can electrochemically exchange Li ions and serve as additional charge-storage sites. [66] Even though this ICE appears similar to the prevalent initial capacity loss in Ge and Si nanomaterial electrodes, oxide contributions prior to reduction to facilitate efficient reversible alloying, are major contributors to the ICE here. The preparation of our GeO_2 IOs via annealing at 450 °C in air may have resulted in similar

Accepted manuscript

ACCEPTED MANUSCRIPT

defect sites which could contribute to the large initial capacity. Since the as-made IO contains nanocrystalline Ge interspersed within the GeO_2 IO matrix, and GeO_2 reduced (detailed further on) to Ge, the large initial coulombic efficiency loss issue of Si and Ge anodes is not as severe in our IO, since part of the charge arises from oxide interactions and GeO_2 reduction. For practical use, particularly in full Li-ion cells, the ICE of the GeO_2 IOs would need to be increased. Low ICE remains an issue for Ge and Si based anode materials however, there are some reports demonstrating that the prelithiation of Si nanostructures via mechanical pressing of Li metal onto the working electrode, in the presence of electrolyte, can improve ICE values. [67, 68]

The first charge curve consists of three distinct regions; a sloping region from 1.5 – 0.85 V, a sloping region from 0.85 – 0.35 V and a long plateau from 0.35 V – 0.01 V. These regions correspond to the formation of amorphous Li_xGeO_2 and the SEI layer, the reduction of Li_xGeO_2 and GeO_2 and the alloying of Ge with Li, respectively. [69] The voltage ranges for each region are in close agreement with the cathodic peaks observed in the first CV scan shown in Figure 3a. The 1st discharge curve consists of 2 sloping regions from 0.3 – 0.7 V and 0.9 – 1.4 V, which correspond to dealloying of Li_xGe and the oxidation of Ge. [59] In the voltage profiles of the 2nd charge to the 50th charge, the voltage gradually decreases from 1.5 to 0.35 V, followed by a long plateau corresponding to the alloying of Ge with Li, however from the 100th to 250th cycles there is a more sudden decrease in potential from 1.5 to 0.35 V. This implies that the processes observed in the initial cycles in this potential range, i.e. the formation of amorphous Li_xGeO_2 and the reduction of Li_xGeO_2 and GeO_2, may no longer occur after ~ 100 cycles and the material reversibly cycles via the alloying and dealloying of Ge with Li. This effect will be further investigated when discussing DCPs obtained from 1000 galvanostatic cycles at a specific current of 300 mA/g. It has previously been reported that irreversible capacity loss (ICL) occurs for many reasons such as the nature of crystal

Accepted manuscript

structure and the particle size of the active material, as well as the typically low operating voltage range used for alloying materials. [70-72]

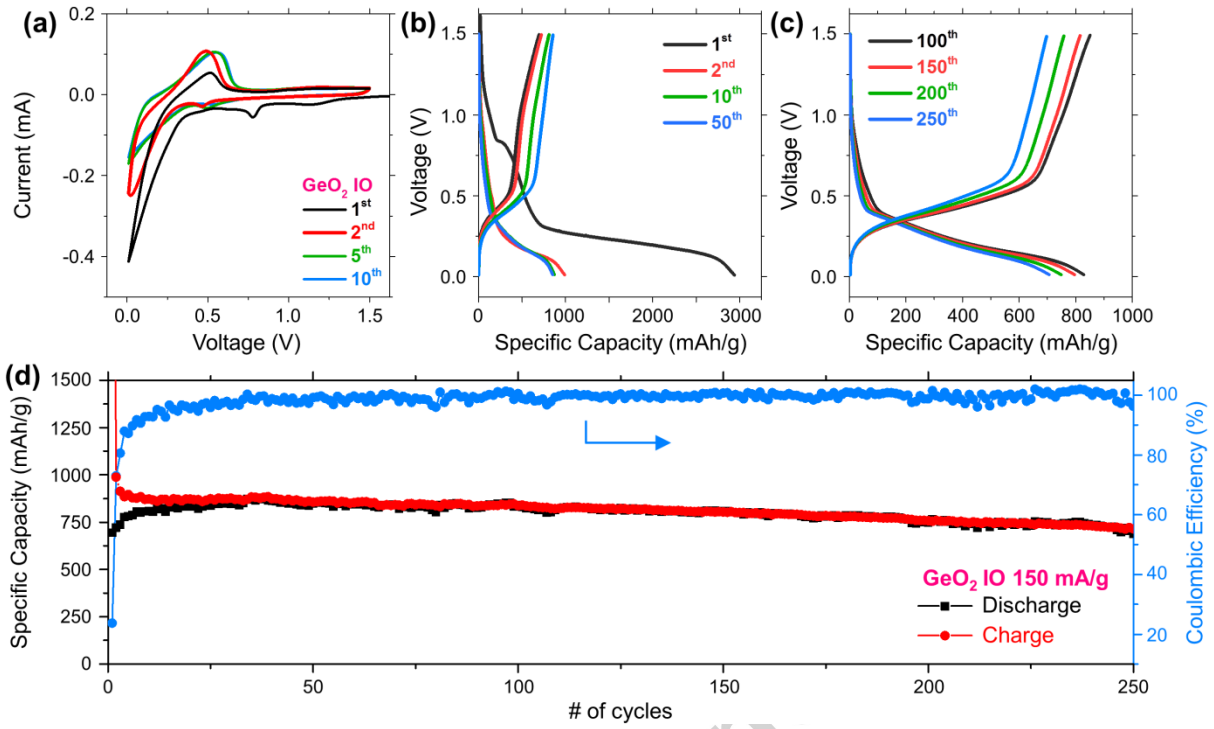

Figure 3. (a) Cyclic voltammograms showing the 1st, 2nd, 5th and 10th cycles, for a GeO_2 IO sample cycled in a potential window from 1.5 – 0.01 V at a scan rate of 0.1 mV/s. Charge and discharge voltage profiles for (b) the 1st, 2nd, 5th,10th and 50th cycles and (c) the 100th, 150th, 200th and 250th cycles for a GeO_2 IO at a specific current of 150 mA/g in a potential window of 1.50 – 0.01 V (vs Li/Li^+). (d) Comparison of the specific capacity values and coulombic efficiency obtained for a GeO_2 IO over 250 cycles.

The specific capacity values obtained over 250 cycles and their related coulombic efficiency values are shown in Figure 3d. GeO_2 IO anodes offer large capacity values with stable capacity retention over 250 cycles. The charge capacity after the 2nd cycle was 988 mAh/g, this decreased to 895 mAh/g after the 5th cycle and decreased slightly to 872 mAh/g after the 10th cycle. From the 10th cycle onwards, the capacity retention is remarkably stable for directly grown, non-slurried IO. The charge capacities after the 100th, 200th and 250th cycles were 836, 757 and 714 mAh/g respectively. The excellent capacity retention is also evident in the stable coulombic efficiency values obtained over 250 cycles. Initial low

Accepted manuscript

ACCEPTED MANUSCRIPT

coulombic efficiencies are common for GeO_2 and alloying anode materials such as Ge and Si [73] and may be attributed to the formation of the SEI layer as well as oxygen defect sites as previously mentioned. However, after the first 10 cycles the coulombic efficiency values were > 95% over the subsequent 240 cycles.

The specific capacity values obtained for our GeO_2 IO anodes are higher than values previously reported for other nanostructured GeO_2 anodes [25, 26, 74-83] and comparable to values reported for pure Ge nanostructures. [73, 84-86] To our knowledge our results represent some the best the electrochemical performances ever reported for nanostructured GeO_2 anodes and composites of GeO_2 and carbon/graphene [79, 81], as demonstrated by the comparison of capacities obtained for various reports of GeO_2 nanostructures shown in Table S2. It is well known that carbon and its various forms actively store charge within the potential range in which GeO_2 is typically cycled. Yoo et al. previously reported on the electrochemical performance of graphite and graphene nanosheets (GNS) cycled in half-cells against Li metal. [87] Both anode materials demonstrated voltage plateaux below 1 V (vs Li/Li^+), which is within the potential range that GeO_2 is cycled in. The reversible capacities for graphite and GNS at a specific current of 50 mA/g were found to be 320 and 540 mAh/g, respectively. This suggests that a portion of the charge stored by composites of GeO_2 with graphene or reduced graphene oxide is likely being stored by graphene. The GeO_2 IOs we show in this work, achieved state of the art response as an anode in the absence of any binders and conductive additives. It is not necessary to prepare composites with graphene to obtain high specific capacities with a stable response from our IO material, and complex oxide reduction to semiconducting Ge, and its associated phase changes via reversible alloying do not alter electronic conductivity nor structural modification that affects cell voltage and energy low during cycling. This represents a significant advancement for nanostructured GeO_2 anode materials.

Accepted manuscript

ACCEPTED MANUSCRIPT

The improved performance is likely due to the inherent porous structure of the IO, which provides a large surface area of material in direct contact with the electrolyte and anchoring to the current collector. It is clear from the stable capacity retention values we observe over the course of hundreds of cycles, shown in Figure 3d, that there is good adhesion of the IO material to the stainless steel substrate. Mechanical adhesion prevents capacity fading from electrically disconnection of material. Previous papers have also discussed the importance of good adhesion between the current collector and active materials. [88, 89] It is well known that Ge undergoes a significant volume expansion as a result of alloying with Li during the charging process. [90, 91] The pores of the IO can accommodate volume changes due to the insertion and removal of Li^+ via expansion into the voids between the walls of the IO. We have previously reported that the electrochemical performance of TiO_2, in terms of capacity values and capacity retention, can be significantly improved by arranging nanoparticles of TiO_2 into a highly ordered, porous, 3D interconnected network in the form of an IO. [45] Likewise, we demonstrate that engineering nanoparticles of GeO_2 into a 3D porous structure significantly improves capacity retention compared to other GeO_2 nanostructures.

To investigate the performance of the GeO_2 IOs at a faster rate, a sample was cycled 1000 times at a specific current of 300 mA/g. A range of the resulting charge and discharge curves over the course of the 1000 cycles are shown in Figure 4a, b and c. The voltage profile for the 1st charge was consistent with the profile observed at the lower specific current of 150 mAh/g, shown in Figure 3b. The charge and discharge capacities after the 1st cycle were 2995 and 689 mAh/g, respectively. This corresponds to an initial Coulombic efficiency of ~23%, which is in close agreement with the initial Coulombic efficiency observed at 150 mA/g (24%). From Figure 4b and c, the voltage profiles are very stable over hundreds of cycles, maintaining a similar charge-discharge curve shape throughout. This stability is also evident

Accepted manuscript

from the capacity values obtained over 1000 cycles. The charge capacity after 50 cycles was 732 mAh/g and this value decreased marginally to 722 mAh/g after 100 cycles. The charge capacity gradually decreased to a value of 657 mAh/g after 300 cycles, 611 mAh/g after 600 cycles and decreased slightly further to 547 mAh/g after 900 cycles. The gradual decrease in specific capacities obtained over the course of 1000 cycles demonstrates the exceptional capacity retention of the GeO_2 IOs.

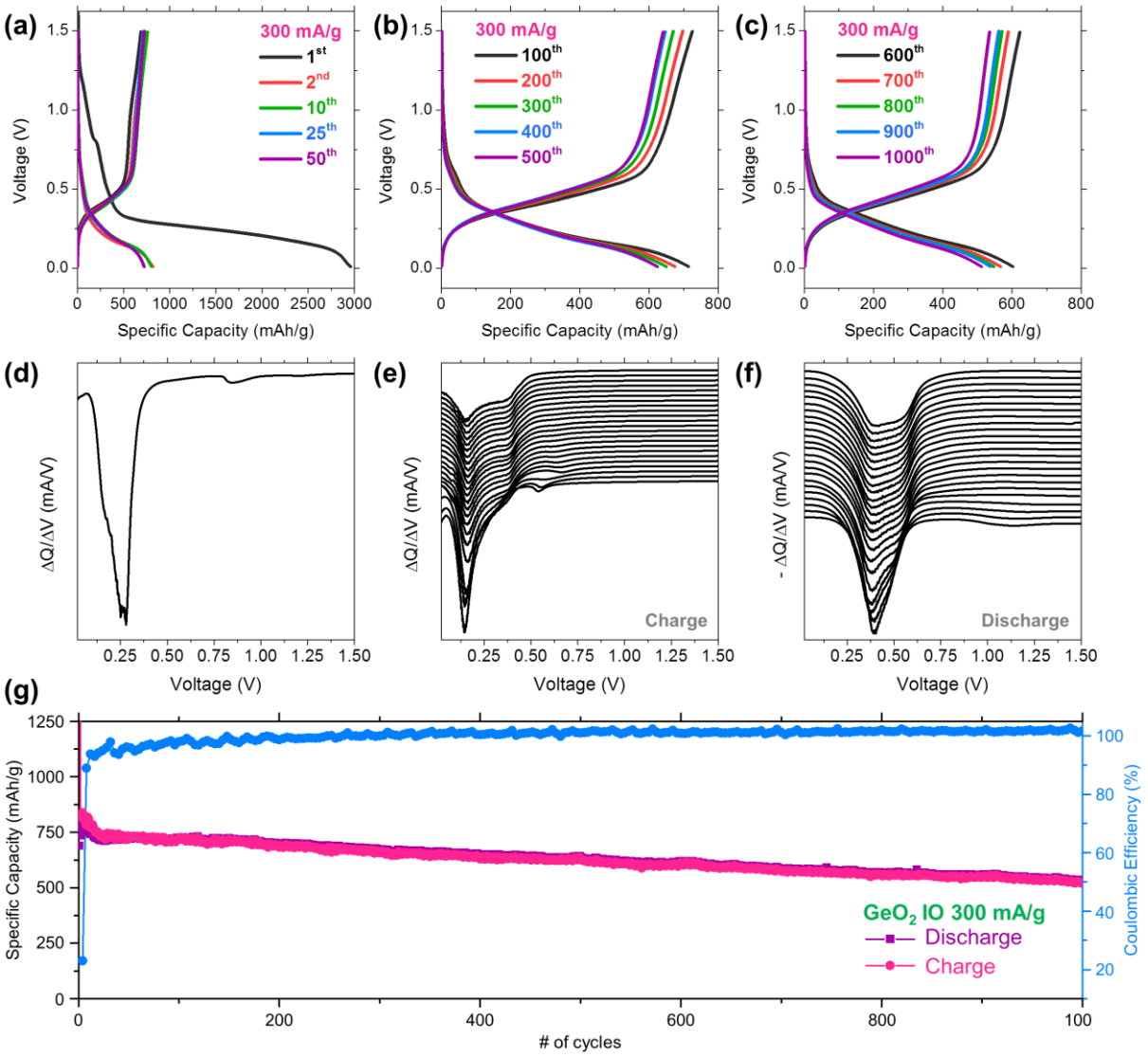

Figure 4. Charge and discharge voltage profiles for (a) the 1st, 2nd, 10th, 25th and 50th cycles, (b) the 100th, 200th, 300th, 400th and 500th cycles and (c) the 600th, 700th, 800th, 900th and 1000th cycles for a GeO_2 IO at a specific current of 300 mA/g in a potential window of 1.50 – 0.01 V (vs Li/Li^+). Differential capacity plots for (d) the 1st charge and (e) a range of charges from the 2nd to the 1000th charge (every 50th curve shown after the 2nd, 5th, and 10th charge). (f) Differential capacity plots for a range of discharges from the 1st to the 1000th discharge

ACCEPTED MANUSCRIPT

(every 50th curve shown after the 1st, 2nd, 5th, and 10th discharge). (g) Comparison of the specific capacity values and coulombic efficiency obtained for a GeO_2 IO over 1000 cycles.

In order to further investigate the electrochemical processes occurring during the 1000 cycle galvanostatic test, DCPs were plotted for a range of charge and discharge curves from the 1st to the 1000th cycle as shown in Figure 4d, e and f. The sharp peak at 0.28 V in the first charge curve is due to the lithiation of crystalline Ge (c-Ge) and was not observed in subsequent cycles. A similar sharp peak at 0.33 V has previously been reported in the first DCP for Ge NWs, which does not reappear in additional cycles. Mullane et al. proposed that the disappearance of this peak indicated that the Ge NWs became completely amorphous upon delithiation. [63] This suggests for our GeO_2 IOs that during the 1st charge, GeO_2 is reduced to c-Ge, which is lithiated at ~0.28 V. From the 2nd cycle onwards the IO samples are reversibly cycled as an alloy with amorphous Ge (a-Ge). The DCP for the 2nd charge consisted of two broad peaks at 0.53 and 0.37 V and a sharp peak at 0.15 V. The two broad peaks can be attributed to the formation of amorphous Li-Ge alloys (a-Li_xGe → a-$Li_{15}Ge_4$) and the sharp peak is due to the formation of c-$Li_{15}Ge_4$. [92, 93] The relative intensities of these three peaks suggests that most of the charge stored in the second charging event is due to the formation of c-$Li_{15}Ge_4$. Over the course of 1000 cycles the relative intensities of these peaks characteristically change in the IO anode. We observe a suppression of the reduction peak associated with c-$Li_{15}Ge_4$ formation, while the differential charge capacity for a-$Li_{15}Ge_4$ increases. This suggests that, with longer cycling, less of the crystalline alloy is formed and consequently a greater proportion of the total charge is stored through the formation of a-$Li_{15}Ge_4$ but importantly, without any adverse effect on the voltage nor capacity fade.

This trend was also observed in the DCPs from the discharge curves, shown in Figure 4f. The DCP for the 1st discharge consisted of a strong, wide asymmetric peak from 0.15 to

Accepted manuscript

ACCEPTED MANUSCRIPT

0.65 V and weak band at 1.15 V. The asymmetric peak can be deconvoluted into two distinct peaks centred at 0.39 and 0.49 V, corresponding to the delithiation of the c-$Li_{15}Ge_4$ and a-$Li_{15}Ge_4$ phases, respectively [94, 95] , as shown in Figure S4. During cycling the intensity of the peak associated with the delithiation of c-$Li_{15}Ge_4$ reduces, giving way to a corresponding increase in the peak associated with the delithiation of a-$Li_{15}Ge_4$. The gradual switch in the relative intensities of these dealloying peaks tracks how the IO anode efficiently maintains reversible Li alloying reactions that cause a crystalline-amorphous phase transition of the alloyed phase, even during modulated Li mole fractions for each charge and discharge portion of extended cycling. This is in close agreement with the observations made in the DCPs for the charging process. The weak band at 1.15 V in the DCP for the 1st discharge is attributed to the oxidation of Ge. [59] This weak band is not observed after the 10th discharge indicating that the oxidation process only occurs for the initial cycles and the IO subsequently cycles reversibly as amorphous Ge. The formation of amorphous and crystalline phases of a Li-Ge alloy is evident from the electrochemical data presented in the DCPs shown in Figure 4 as well as in Figures S5, S6 and S7.

The specific capacity values obtained over 1000 cycles at a specific current of 300 mA/g and the corresponding coulombic efficiencies are shown in Figure 4g. The specific capacity after the 2nd charge was ~830 mAh/g and after 20 cycles this decreased to ~740 mAh/g. From the 20th cycle onwards there was a significant increase in the capacity retention and the decrease in capacities became far more gradual. We propose that the increased stability is due to the complete reduction of GeO_2 over a number of cycles and the subsequent cycling of amorphous Ge, in a material that is structured to accommodate associated material volume changes in binder-free format. The GeO_2 IO demonstrated impressive stable capacity retention when cycled at a specific current of 300 mA/g retaining capacities of 682, 632 and 521 mAh/g after the 200th, 500th and 1000th cycles respectively. These values correspond to

Accepted manuscript

ACCEPTED MANUSCRIPT

capacity retentions of 82%, 76% and 63% from the 2nd cycle at relatively high rate. Retaining such a high level of capacity even after 500 and 1000 cycles clearly demonstrates the viability of the GeO_2 IOs for use as an anode material in practical commercial full Li-ion cells. The average charge capacity for the GeO_2 IO over 1000 cycles was ~630 mAh/g. This useful capacity retention characteristic of easily processed GeO_2 IO is also evident in the Coulombic efficiency values obtained over 1000 cycles. Similar to the galvanostatic cycling test at 150 mA/g, the initial Coulombic efficiency is characteristically low but after 10 cycles the Coulombic efficiency is >95% and remarkably remains above this value for the remainder of the 1000 cycles.

The high-rate performance of GeO_2 IO samples was further investigated by rate capability testing using a series of different specific currents ranging from 250 – 1000 mA/g. It is immediately clear from the resulting specific capacities in Figure 5a that the GeO_2 IOs provide outstanding rate capability performance (compare to Table S2). The specific capacity obtained after 20 cycles at a specific current of 250 mA/g was ~ 685 mAh/g. The average capacity obtained at a specific current of 500 mA/g was ~616 mAh/g, this decreased slightly to 591 mAh/g at 750 mA/g, and decreased slightly further to 576 mAh/g at 1000 mA/g. When the specific current was returned to the initial value of 250 mA/g the specific capacity recovered to 636 mAh/g after the 81st charge and increased further to 706 mAh/g after the 82nd charge. From the specific capacity values obtained from galvanostatic testing, presented in Figure 3d and Figure 4g, as well as from the rate capability test shown in Figure 5a it is clear that the GeO_2 IO anodes demonstrate significant reversible capacity with consistent and stable capacity retention. GeO_2 IO samples offer increased capacity retention compared to previously reported rate test performances of other GeO_2 nanostructures, cycled at similar specific currents/ C-rates. [24, 25]

Accepted manuscript

ACCEPTED MANUSCRIPT

The rate capability test demonstrates the ability of GeO_2 IO samples to deliver significantly high capacities even at a high specific current (1000 mA/g). To further investigate the high rate performance of the GeO_2 IOs, a sample was galvanostatically cycled asymmetrically, mimicking 'quick charging and normal use' of a battery. The IO sample was charged with a specific current of 300 mA/g and discharged with a specific current of 1000 mA/g. A selection of the resulting charge and discharge curves over 200 cycles are shown in Figure 5b and c. The initial charge and discharge capacities were 3219 and 479 mAh/g, respectively. This corresponds to an initial Coulombic efficiency of ~ 15%, which is lower than the efficiency obtained when charged and discharged at 300 mA/g (23%). The lower initial efficiency is most likely due the asymmetry in the specific current used for charging and discharging. The specific capacity after the 2^{nd} charge was 627 mAh/g and this decreased to 551 mAh/g after the 10^{th} charge. From the 10^{th} cycle onwards the capacity retention was significantly improved, with the IO sample demonstrating charge capacities of 524 and 508 mAh/g after the 50^{th} and 150^{th} cycles, respectively. The capacity values obtained during the asymmetric test are lower that the galvanostatic test performed at 300 mA/g, (Figure 4) however the capacity retention is just as impressive. Analysis of DCPs will be used to determine the reason for this decrease in specific capacity values.

As Li-ion battery anodes typically undergo asymmetric charging and discharging during daily use, we investigated the effect of fast discharging of the anode following relatively slow charging. In parallel, we assessed the influence of this asymmetry cycling profile on the alloying/dealloying processes. The same specific current used for the test shown in Figure 4 (300 mA/g) was applied to charge the anode, and a larger specific current of 1000 mA/g was used during discharging (note: discharging an anode is opposite to the cathode, i.e. from low to high voltage). To determine the effect of charging at a higher specific current on the lithiation/delithiation processes, DCPs were plotted from the

Accepted manuscript

ACCEPTED MANUSCRIPT

asymmetric charge and discharge curves from Figure 5b and c. The resulting DCPs are shown in Figures S5. The DCP for the first charge curve contains a sharp peak at 0.27 V which is attributed to the lithiation of c-Ge and this peak was not observed in from the 2nd cycle onwards. This is in close agreement with the DCP shown in Figure 4d which was determined from a GeO_2 IO also charged at a specific current of 300 mA/g. This demonstrates the consistency of the electrochemical response of the GeO_2 IOs. The remaining DCPs from charging at 300 mA/g are also in excellent agreement with the curves presented in Figure 4e. From the 2nd charge onwards, the DCPs consist of two peaks at 0.35 V and 0.15 V, corresponding to the formation of a-$Li_{15}Ge_4$ and c-$Li_{15}Ge_4$, respectively. With increased cycling, the data confirms that the dominant phase for charge storage switched from c-$Li_{15}Ge_4$ to a-$Li_{15}Ge_4$.

Accepted manuscript

ACCEPTED MANUSCRIPT

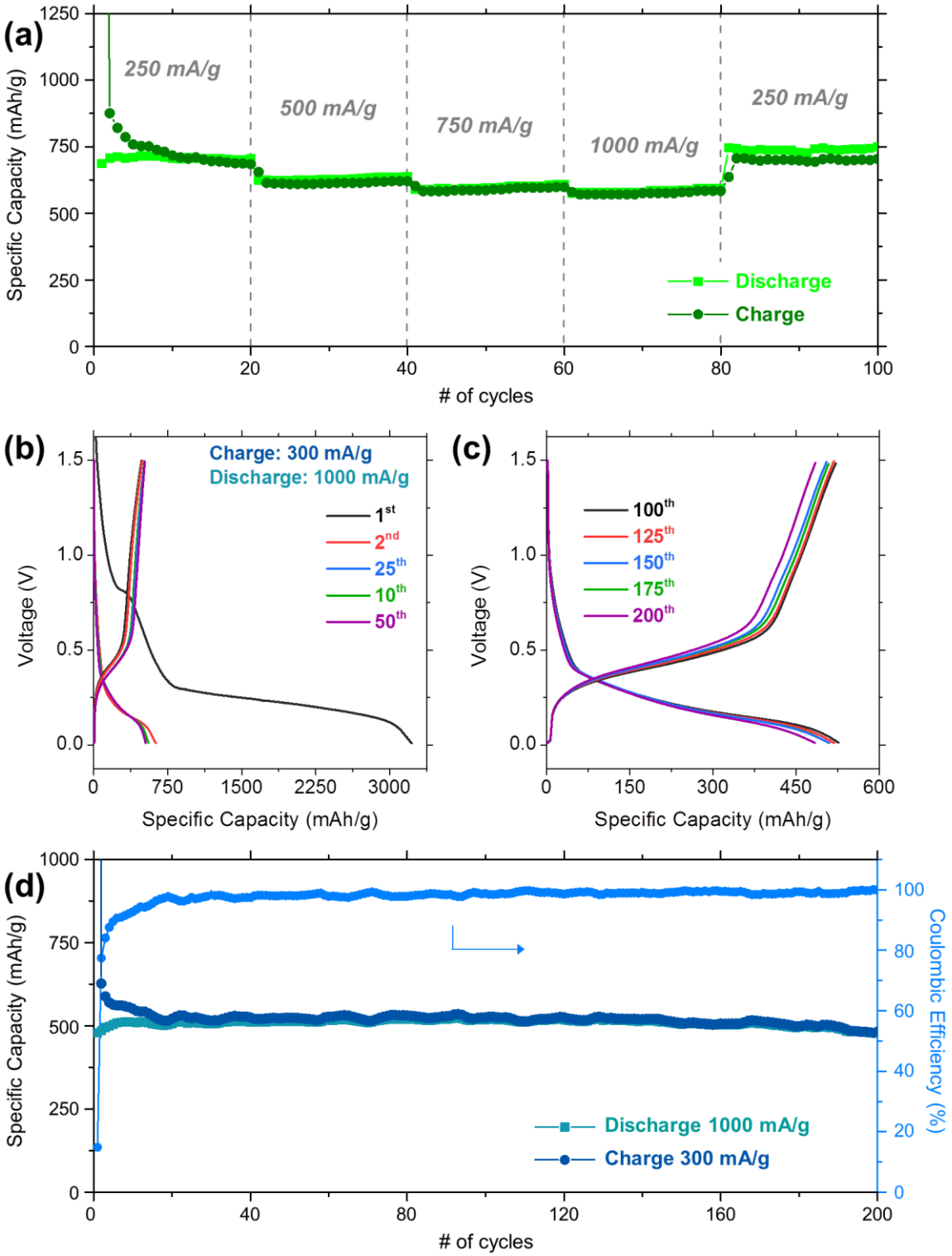

Figure 5. (a) Rate capability test for a GeO_2 IO over 100 cycles, using specific currents ranging from 250 to 1000 mA/g. (b) Charge and discharge voltage profiles for (b) the 1st, 2nd, 10th, 25th and 50th cycles, (c) the 100th, 125th, 150th, 175th and 200th cycles for a GeO_2 IO charged at a specific current of 300 mA/g and discharged at a specific current of 1000 mA/g, in a potential window of 1.50 – 0.01 V (vs Li/Li$^+$). (d) Comparison of the specific capacity values and coulombic efficiency obtained for a GeO_2 IO cycled asymmetrically over 200 cycles.

ACCEPTED MANUSCRIPT

The DCPs determined from the charge curves obtained at a specific current of 300 mA/g are in close agreement with those presented in Figure 4d and e, however there is a significant difference in the DCPs determined from the discharge curves. The DCP for the 1st discharge at 300 mA/g shown in Figure S4 consists of 2 peaks centred at ~ 0.40 and 0.50 V, corresponding to the delithiation of the c-$Li_{15}Ge_4$ and a-$Li_{15}Ge_4$ phases, respectively. However, the DCP for the 1st charge at 1000 mA/g, shown in Figure S5c, consists of only one peak at 0.40 V, implying that only the c-$Li_{15}Ge_4$ phase was delithiated. To further investigate this, the wide peak from 0.01 to 0.75 V, present in each of the DCPs for the discharge curves, was deconvoluted and the resulting fitted peaks are shown in Figure S6 and S7. It can be clearly seen in Figure S6a and b, that the peak associated with the delithiation of the a-$Li_{15}Ge_4$ phase is not present in the DCPs for the first two discharges. This explains why the initial Coulombic efficiency for the asymmetric test was lower than the other galvanostatic tests and may also explain why the specific capacities are lower also. By not fully delithiating the a-$Li_{15}Ge_4$ phase, during discharging, less charge will be stored in subsequent cycles and consequently the specific capacities are suppressed. From Figure S6c a weak peak associated with the delithiation of the a-$Li_{15}Ge_4$ phase was observed from the 10th cycle onwards and the intensity of this peak increased with additional cycling, as shown in Figure S7. The DCPs demonstrate that both the c-$Li_{15}Ge_4$ and a-$Li_{15}Ge_4$ phases are formed during charging at 300 mA/g, however, initially only the c-$Li_{15}Ge_4$ phase is delithiated during discharge at the higher specific current of 1000 mA/g, resulting in lower specific capacity values than those obtained via standard symmetric galvanostatic cycling. SEM images of GeO_2 IO samples after 250 galvanostatic cycles using a specific current of 150 mA/g and after 1000 cycles using a specific current of 300 mA/g are shown in Figure S8. After long term cycling the overall IO morphology no longer remains, which, is most likely due to reduction of the initial GeO_2 IO

Accepted manuscript

ACCEPTED MANUSCRIPT

to GeO and Ge metal and the repeated alloying of Ge with Li over the course of hundreds of cycles.

The specific capacity values obtained over 200 cycles from asymmetric cycling and the related coulombic efficiencies are shown in Figure 5d. As previously mentioned, the capacity retention of the GeO_2 IO was significantly improved from the ~10^{th} cycle onwards, with a more gradual decrease in capacity values observed from that point. The specific capacities after the 100^{th} and 200^{th} charges were ~524 and 480 mAh/g respectively, corresponding to a capacity retention of ~95 and 87% from the 10^{th} charge. This demonstrates that even when cycled asymmetrically the GeO_2 IOs maintain an impressively high level of capacity retention. The stable capacity retention is also observed in the Coulombic efficiency values obtained over 200 cycles. The initial efficiencies are <90%, possibly due to lack of the delithiation of the a-$Li_{15}Ge_4$ phase over the first few cycles. However, from the 10^{th} cycle onwards the Coulombic efficiency is > 95% and remains above this value for the remainder of the 200 cycles.

In summary, GeO_2 IOs were prepared via thermal treatment of a sacrificial PS sphere template which was infilled with a germanium ethoxide solution. The hexagonal crystal structure of our GeO_2 IO samples was confirmed via XRD and ED. Raman, XPS and PL analysis indicates that there is some metallic Ge present in the IO samples, possibly in the form of Ge nanocrystals embedded in a GeO_2 matrix. Galvanostatic cycling at a specific current of 150 mA/g demonstrated the exceptional capacity retention properties of the GeO_2 IOs, achieving a reversible capacity of ~ 856 and 714 mAh/g after the 50^{th} and 250^{th} cycles respectively. These values are greater than previously reported values for other GeO_2 nanostructures and comparable to values obtained from pure Ge nanostructures. The long cycle life performance of the GeO_2 IOs was investigated by galvanostatic cycling with a specific current of 300 mA/g for 1000 cycles. The excellent stability of the GeO_2 IO samples

Accepted manuscript

ACCEPTED MANUSCRIPT

was evident again from the capacity values obtained during cycling. The specific capacities after the 500th and 1000th cycles were 632 and 521 mAh/g respectively, corresponding to capacity retentions of 76 and 63% from the 2nd cycle.

Rate capability testing demonstrated the ability of the GeO_2 IOs to deliver large reversible capacities when cycled using high specific currents (1000 mA/g), with tolerance to cumulatively higher rates with minimal capacity fading. The high rate performance of the GeO_2 IO samples was further evaluated through asymmetric galvanostatic cycling. GeO_2 IOs demonstrated large stable capacities (~500 mAh/g) over 200 cycles when discharged at a specific current that was >3× the specific current used to charge the anode. DCPs were used to investigate the differences in charge storage when GeO_2 IOs are cycled asymmetrically compared to standard galvanostatic cycling. It was determined that at faster rates, initially only the c-$Li_{15}Ge_4$ phase is delithiated during discharge, resulting in lower specific capacity values than those obtained via standard galvanostatic cycling.

The specific capacity results presented in this report, to our knowledge, represent one of the best the electrochemical performances ever reported for GeO_2. Additionally, the impressive electrochemical performance of our GeO_2 IO samples was achieved in the absence of any binders or conductive additives. We propose that the superior specific capacities and capacity retention obtained with the GeO_2 IOs are due to the initial highly porous, complex, 3D interconnected network, which is a characteristic of the IO structure, and this structure ensure an structurally stable, interconnected material that facilities efficiency alloying reaction with the nanoparticulate walls of the IO structure to boost Coulombic efficiency. GeO_2 IOs are a Ge-based anode material, which can be prepared in air with cost effective precursors, without the need for an inert atmosphere or any additional processing steps, such as the preparation of a slurry, which can deliver capacity values and retention greater than other GeO_2 nanostructures and comparable to pure Ge nanostructures.

Accepted manuscript

ACCEPTED MANUSCRIPT

The impressive electrochemical performance of the GeO_2 IOs in terms of specific capacities, capacity retention and voltage stability over 1000 cycles demonstrates that they are a very promising anode material for long cycle life Li-ion batteries.

Supplementary material

Experimental details for the preparation of GeO_2 IO samples and for the structural and electrochemical characterization. TEM images showing the walls of the GeO_2 IO samples consist of nanoparticles. Deconvoluted anodic scan from the first CV scan for GeO_2 IO cycled in a potential window from 1.5 – 0.01 V (vs Li/Li^+) at a scan rate of 0.1 mV/s. DCPs from galvanostatic cycling with a specific current of 150 mA/g and 300 mAh/g and from asymmetric charge-discharge testing. The asymmetric testing consisted of charging with a specific current of 300 mA/g and discharging with a specific current of 1000 mA/g.

Notes

The authors declare no competing financial interest.

Accepted manuscript

ACKNOWLEDGMENTS

This work was also supported by Science Foundation Ireland (SFI) through SFI Technology Innovation & Development Awards under contract no. 13/TIDA/E2761 and 15/TIDA/2893. This publication was also supported by the Royal Irish Academy under the Charlemont Grant. This publication has also emanated from research supported in part by a research grant from SFI under Grant Number 14/IA/2581 and from the Irish Research Council Government of Ireland Postgraduate Award under contract GOIPG/2014/206.

ACCEPTED MANUSCRIPT

References

[1] B. Dunn, H. Kamath, J.-M. Tarascon, Electrical Energy Storage for the Grid: A Battery of Choices, Science 334 (2011) 928-935.

[2] J.B. Goodenough, K.-S. Park, The Li-Ion Rechargeable Battery: A Perspective, J. Am. Chem. Soc. 135 (2013) 1167-1176.

[3] C.P. Grey, J.M. Tarascon, Sustainability and in situ monitoring in battery development, Nat. Mater. 16 (2017) 45-56.

[4] D. Larcher, J.M. Tarascon, Towards greener and more sustainable batteries for electrical energy storage, Nat. Chem. 7 (2015) 19-29.

[5] D. McNulty, Q. Ramasse, C. O'Dwyer, The structural conversion from α-$AgVO_3$ to β-$AgVO_3$: Ag nanoparticle decorated nanowires with application as cathode materials for Li-ion batteries, Nanoscale 8 (2016) 16266-16275.

[6] D. McNulty, D.N. Buckley, C. O'Dwyer, Polycrystalline Vanadium Oxide Nanorods: Growth, Structure and Improved Electrochemical Response as a Li-Ion Battery Cathode Material, J. Electrochem. Soc. 161 (2014) A1321-A1329.

[7] N. Nitta, F. Wu, J.T. Lee, G. Yushin, Li-ion battery materials: present and future, Mater. Today 18 (2015) 252-264.

[8] J.W. Choi, D. Aurbach, Promise and reality of post-lithium-ion batteries with high energy densities, Nat. Rev. Mater. 1 (2016) 16013.

[9] M.V. Reddy, G.V. Subba Rao, B.V.R. Chowdari, Metal Oxides and Oxysalts as Anode Materials for Li Ion Batteries, Chem. Rev. 113 (2013) 5364-5457.

[10] M.V. Reddy, G.V. Subba Rao, B.V.R. Chowdari, Nano-$(V_{1/2}Sb_{1/2}Sn)O_4$: a high capacity, high rate anode material for Li-ion batteries, J. Mater. Chem. 21 (2011) 10003-10011.

[11] M.V. Reddy, G.V. Subba Rao, B.V.R. Chowdari, Li-storage and cycling properties of Sn–Sb-mixed oxides, $(M_{1/2}Sb_{1/2}Sn)O_4$, M = In, Fe, J. Solid State Electrochem. 17 (2013) 1765-1773.

[12] A.K. Jibin, M.V. Reddy, G.V. Subba Rao, U.V. Varadaraju, B.V.R. Chowdari, Pb_3O_4 type antimony oxides MSb_2O_4 (M=Co, Ni) as anode for Li-ion batteries, Electrochim. Acta 71 (2012) 227-232.

[13] P. Nithyadharseni, M.V. Reddy, B. Nalini, T.R. Ravindran, B.C. Pillai, M. Kalpana, B.V.R. Chowdari, Electrochemical studies of CNT/Si–SnSb nanoparticles for lithium ion batteries, Mater. Res. Bull. 70 (2015) 478-485.

[14] C.T. Cherian, M. Zheng, M.V. Reddy, B.V.R. Chowdari, C.H. Sow, Zn_2SnO_4 Nanowires versus Nanoplates: Electrochemical Performance and Morphological Evolution during Li-Cycling, ACS Appl. Mater. Interfaces 5 (2013) 6054-6060.

[15] T. Song, H. Cheng, H. Choi, J.-H. Lee, H. Han, D.H. Lee, D.S. Yoo, M.-S. Kwon, J.-M. Choi, S.G. Doo, H. Chang, J. Xiao, Y. Huang, W.I. Park, Y.-C. Chung, H. Kim, J.A. Rogers, U. Paik, Si/Ge Double-Layered Nanotube Array as a Lithium Ion Battery Anode, ACS Nano 6 (2012) 303-309.

Accepted manuscript

ACCEPTED MANUSCRIPT

[16] Z. Hu, S. Zhang, C. Zhang, G. Cui, High performance germanium-based anode materials, Coord. Chem. Rev. 326 (2016) 34-85.

[17] C.K. Chan, X.F. Zhang, Y. Cui, High Capacity Li Ion Battery Anodes Using Ge Nanowires, Nano Lett. 8 (2008) 307-309.

[18] D.-J. Xue, S. Xin, Y. Yan, K.-C. Jiang, Y.-X. Yin, Y.-G. Guo, L.-J. Wan, Improving the Electrode Performance of Ge through Ge@C Core–Shell Nanoparticles and Graphene Networks, J. Am. Chem. Soc. 134 (2012) 2512-2515.

[19] X. Xiao, X. Li, S. Zheng, J. Shao, H. Xue, H. Pang, Nanostructured Germanium Anode Materials for Advanced Rechargeable Batteries, Adv. Mater. Inter. 4 (2017) DOI: 10.1002/admi.201600798.

[20] D. Li, H. Wang, H.K. Liu, Z. Guo, A New Strategy for Achieving a High Performance Anode for Lithium Ion Batteries—Encapsulating Germanium Nanoparticles in Carbon Nanoboxes, Adv. Energy Mater. 6 (2016) 1501666.

[21] D. Li, H. Wang, T. Zhou, W. Zhang, H.K. Liu, Z. Guo, Unique Structural Design and Strategies for Germanium-Based Anode Materials Toward Enhanced Lithium Storage, Adv. Energy Mater. (2017) DOI:10.1002/aenm.201700488.

[22] M.-H. Park, Y. Cho, K. Kim, J. Kim, M. Liu, J. Cho, Germanium Nanotubes Prepared by Using the Kirkendall Effect as Anodes for High-Rate Lithium Batteries, Angew. Chem. 123 (2011) 9821-9824.

[23] L. Ma, E. Fahrenkrug, E. Gerber, A.J. Crowe, F. Venable, B.M. Bartlett, S. Maldonado, High-Performance Polycrystalline Ge Microwire Film Anodes for Li Ion Batteries, ACS Energy Lett. 2 (2017) 238-243.

[24] Y. Son, M. Park, Y. Son, J.-S. Lee, J.-H. Jang, Y. Kim, J. Cho, Quantum Confinement and Its Related Effects on the Critical Size of GeO_2 Nanoparticles Anodes for Lithium Batteries, Nano Lett. 14 (2014) 1005-1010.

[25] Y.-M. Lin, K.C. Klavetter, A. Heller, C.B. Mullins, Storage of Lithium in Hydrothermally Synthesized GeO_2 Nanoparticles, J. Phys. Chem. Lett. 4 (2013) 999-1004.

[26] A. Jahel, A. Darwiche, C. Matei Ghimbeu, C. Vix-Guterl, L. Monconduit, High cycleability nano-GeO_2/mesoporous carbon composite as enhanced energy storage anode material in Li-ion batteries, J. Power Sources 269 (2014) 755-759.

[27] E. Armstrong, C. O'Dwyer, Artificial opal photonic crystals and inverse opal structures - fundamentals and applications from optics to energy storage, J. Mater. Chem. C 3 (2015) 6109-6143.

[28] H. Liu, H.-M. Cho, Y.S. Meng, Q. Li, Engineering Three-Dimensionally Electrodeposited Si-on-Ni Inverse Opal Structure for High Volumetric Capacity Li-Ion Microbattery Anode, ACS Appl. Mater. Interfaces 6 (2014) 9842-9849.

[29] G. Collins, E. Armstrong, D. McNulty, S. O'Hanlon, H. Geaney, C. O'Dwyer, 2D and 3D photonic crystal materials for photocatalysis and electrochemical energy storage and conversion, Sci. Tech. Adv. Mater. 17 (2016) 563-582.

[30] C. O'Dwyer, Color-Coded Batteries – Electro-Photonic Inverse Opal Materials for Enhanced Electrochemical Energy Storage and Optically Encoded Diagnostics, Adv. Mater. 28 (2016) 5681-5688.

Accepted manuscript

ACCEPTED MANUSCRIPT

[31] J. Liu, Q. Zheng, M.D. Goodman, H. Zhu, J. Kim, N.A. Krueger, H. Ning, X. Huang, J. Liu, M. Terrones, P.V. Braun, Graphene Sandwiched Mesostructured Li-Ion Battery Electrodes, Adv. Mater. 28 (2016) 7696-7702.

[32] J.H. Pikul, H.G. Zhang, J. Cho, P.V. Braun, W.P. King, High-power lithium ion microbatteries from interdigitated three-dimensional bicontinuous nanoporous electrodes, Nat. Commun. 4 (2013) 1732.

[33] H. Ning, J.H. Pikul, R. Zhang, X. Li, S. Xu, J. Wang, J.A. Rogers, W.P. King, P.V. Braun, Holographic patterning of high-performance on-chip 3D lithium-ion microbatteries, Proc. Natl. Acad. Sci. U.S.A. 112 (2015) 6573-6578.

[34] S. O'Hanlon, D. McNulty, C. O'Dwyer, The Influence of Colloidal Opal Template and Substrate Type on 3D Macroporous Single and Binary Vanadium Oxide Inverse Opal Electrodeposition, J. Electrochem. Soc. 164 (2017) D111-D119.

[35] H. Zhang, X. Yu, P.V. Braun, Three-dimensional bicontinuous ultrafast-charge and -discharge bulk battery electrodes, Nat. Nanotechnol. 6 (2011) 277-281.

[36] A. Vu, Y. Qian, A. Stein, Porous Electrode Materials for Lithium-Ion Batteries – How to Prepare Them and What Makes Them Special, Adv. Energy Mater. 2 (2012) 1056-1085.

[37] J. Zhu, R. Duan, S. Zhang, N. Jiang, Y. Zhang, J. Zhu, The application of graphene in lithium ion battery electrode materials, SpringerPlus 3 (2014) 585.

[38] Y.-K. Sun, S.-T. Myung, B.-C. Park, J. Prakash, I. Belharouak, K. Amine, High-energy cathode material for long-life and safe lithium batteries, Nat. Mater. 8 (2009) 320-324.

[39] Y.-K. Sun, Z. Chen, H.-J. Noh, D.-J. Lee, H.-G. Jung, Y. Ren, S. Wang, C.S. Yoon, S.-T. Myung, K. Amine, Nanostructured high-energy cathode materials for advanced lithium batteries, Nat. Mater. 11 (2012) 942-947.

[40] D. Lin, Y. Liu, Y. Cui, Reviving the lithium metal anode for high-energy batteries, Nat. Nanotechnol. 12 (2017) 194-206.

[41] A. Basile, A.I. Bhatt, A.P. O'Mullane, Stabilizing lithium metal using ionic liquids for long-lived batteries, Nat. Commun. 7 (2016) 11794.

[42] M. Osiak, H. Geaney, E. Armstrong, C. O'Dwyer, Structuring materials for lithium-ion batteries: advancements in nanomaterial structure, composition, and defined assembly on cell performance, J. Mater. Chem. A 2 (2014) 9433-9460.

[43] E. Armstrong, D. McNulty, H. Geaney, C. O'Dwyer, Electrodeposited Structurally Stable V_2O_5 Inverse Opal Networks as High Performance Thin Film Lithium Batteries, ACS Appl. Mater. Interfaces 7 (2015) 27006-27015.

[44] D. McNulty, H. Geaney, E. Armstrong, C. O'Dwyer, High performance inverse opal Li-ion battery with paired intercalation and conversion mode electrodes, J. Mater. Chem. A 4 (2016) 4448-4456.

[45] D. McNulty, G. Hugh, C. Elaine, G. Shane, L. Alex, O.D. Colm, The effect of particle size, morphology and C-rates on 3D structured Co_3O_4 inverse opal conversion mode anode materials, Mater. Res. Express 4 (2017) 025011.

Accepted manuscript

ACCEPTED MANUSCRIPT

[46] D. McNulty, H. Geaney, C. O'Dwyer, Carbon-Coated Honeycomb Ni-Mn-Co-O Inverse Opal: A High Capacity Ternary Transition Metal Oxide Anode for Li-ion Batteries, Sci. Rep. 7 (2017) 42263.

[47] S.P. Mukherjee, S.K. Sharma, A comparative Raman study of the structures of conventional and gel-derived glasses in the SiO_2-GeO_2 system, J. Non-Cryst. Solids 71 (1985) 317-325.

[48] P. Gillet, A. Le Cléac'h, M. Madon, High-temperature raman spectroscopy of SiO_2 and GeO_2 Polymorphs: Anharmonicity and thermodynamic properties at high-temperatures, J. Geophys. Res. B: Solid Earth 95 (1990) 21635-21655.

[49] P.K.G.a.S. Dhara, Freestanding Ge/GeO_2 Core-Shell Nanocrystals with Varying Sizes and Shell Thicknesses: Microstructure and Photoluminescence Studies, J. Nanomater. 2012 (2012).

[50] S.K. Sharma, D. Virgo, I. Kushiro, Relationship between density, viscosity and structure of GeO_2 melts at low and high pressures, J. Non-Cryst. Solids 33 (1979) 235-248.

[51] Z. Sui, I.P. Herman, Effect of strain on phonons in Si, Ge, and Si/Ge heterostructures, Phys. Rev. B 48 (1993) 17938-17953.

[52] K. Prabhakaran, T. Ogino, Oxidation of Ge(100) and Ge(111) surfaces: an UPS and XPS study, Surf. Sci. 325 (1995) 263-271.

[53] L.T. Canham, Silicon quantum wire array fabrication by electrochemical and chemical dissolution of wafers, Appl. Phys. Lett. 57 (1990) 1046-1048.

[54] B.R. Taylor, S.M. Kauzlarich, G.R. Delgado, H.W.H. Lee, Solution Synthesis and Characterization of Quantum Confined Ge Nanoparticles, Chem. Mater. 11 (1999) 2493-2500.

[55] O. Millo, I. Balberg, D. Azulay, T.K. Purkait, A.K. Swarnakar, E. Rivard, J.G.C. Veinot, Direct Evaluation of the Quantum Confinement Effect in Single Isolated Ge Nanocrystals, J. Phys. Chem. Lett. 6 (2015) 3396-3402.

[56] X. Zou, B. Liu, Q. Li, Z. Li, B. Liu, W. Wu, Q. Zhao, Y. Sui, D. Li, B. Zou, T. Cui, G. Zou, H.-K. Mao, One-step synthesis, growth mechanism and photoluminescence properties of hollow GeO_2 walnuts, CrystEngComm 13 (2011) 979-984.

[57] G. Kartopu, S.C. Bayliss, R.E. Hummel, Y. Ekinci, Simultaneous micro-Raman and photoluminescence study of spark-processed germanium: Report on the origin of the orange photoluminescence emission band, J. Appl. Phys. 95 (2004) 3466-3472.

[58] J.S. Peña, I. Sandu, O. Joubert, F.S. Pascual, C.O. Areán, T. Brousse, Electrochemical Reaction Between Lithium and β-Quartz GeO_2, Electrochem. Solid State Lett. 7 (2004) A278-A281.

[59] H. Qiu, L. Zeng, T. Lan, X. Ding, M. Wei, In situ synthesis of GeO_2/reduced graphene oxide composite on Ni foam substrate as a binder-free anode for high-capacity lithium-ion batteries, J. Mater. Chem. A 3 (2015) 1619-1623.

[60] L. Mei, M. Mao, S. Chou, H. Liu, S. Dou, D.H.L. Ng, J. Ma, Nitrogen-doped carbon nanofibers with effectively encapsulated GeO_2 nanocrystals for highly reversible lithium storage, J. Mater. Chem. A 3 (2015) 21699-21705.

Accepted manuscript

ACCEPTED MANUSCRIPT

[61] Y. Chen, C. Yan, O.G. Schmidt, Strain-Driven Formation of Multilayer Graphene/GeO_2 Tubular Nanostructures as High-Capacity and Very Long-Life Anodes for Lithium-Ion Batteries, Adv. Energy Mater. 3 (2013) 1269-1274.

[62] S. Yoon, S.-H. Jung, K.-N. Jung, S.-G. Woo, W. Cho, Y.-N. Jo, K.Y. Cho, Preparation of nanostructured Ge/GeO_2 composite in carbon matrix as an anode material for lithium-ion batteries, Electrochim. Acta 188 (2016) 120-125.

[63] E. Mullane, T. Kennedy, H. Geaney, K.M. Ryan, A Rapid, Solvent-Free Protocol for the Synthesis of Germanium Nanowire Lithium-Ion Anodes with a Long Cycle Life and High Rate Capability, ACS Appl. Mater. Interfaces 6 (2014) 18800-18807.

[64] L.Y. Lim, N. Liu, Y. Cui, M.F. Toney, Understanding Phase Transformation in Crystalline Ge Anodes for Li-Ion Batteries, Chem. Mater. 26 (2014) 3739-3746.

[65] D.T. Ngo, R.S. Kalubarme, H.T.T. Le, C.-N. Park, C.-J. Park, Conducting additive-free amorphous GeO_2/C composite as a high capacity and long-term stability anode for lithium ion batteries, Nanoscale 7 (2015) 2552-2560.

[66] K.E. Swider-Lyons, C.T. Love, D.R. Rolison, Improved lithium capacity of defective V_2O_5 materials, Solid State Ion. 152–153 (2002) 99-104.

[67] N. Liu, L. Hu, M.T. McDowell, A. Jackson, Y. Cui, Prelithiated Silicon Nanowires as an Anode for Lithium Ion Batteries, ACS Nano 5 (2011) 6487-6493.

[68] M.W. Forney, M.J. Ganter, J.W. Staub, R.D. Ridgley, B.J. Landi, Prelithiation of Silicon–Carbon Nanotube Anodes for Lithium Ion Batteries by Stabilized Lithium Metal Powder (SLMP), Nano Lett. 13 (2013) 4158-4163.

[69] L. Zeng, X. Huang, X. Chen, C. Zheng, Q. Qian, Q. Chen, M. Wei, Ge/GeO_2-Ordered Mesoporous Carbon Nanocomposite for Rechargeable Lithium-Ion Batteries with a Long-Term Cycling Performance, ACS Appl. Mater. Interfaces 8 (2016) 232-239.

[70] M.V. Reddy, C. Yu, F. Jiahuan, K.P. Loh, B.V.R. Chowdari, Li-Cycling Properties of Molten Salt Method Prepared Nano/Submicrometer and Micrometer-Sized CuO for Lithium Batteries, ACS Appl. Mater. Interfaces 5 (2013) 4361-4366.

[71] M.V. Reddy, B.L. Wei Wen, K.P. Loh, B.V.R. Chowdari, Energy Storage Studies on $InVO_4$ as High Performance Anode Material for Li-Ion Batteries, ACS Appl. Mater. Interfaces 5 (2013) 7777-7785.

[72] M.V. Reddy, L.Y.T. Andreea, A.Y. Ling, J.N.C. Hwee, C.A. Lin, S. Admas, K.P. Loh, M.K. Mathe, K.I. Ozoemena, B.V.R. Chowdari, Effect of preparation temperature and cycling voltage range on molten salt method prepared SnO_2, Electrochim. Acta 106 (2013) 143-148.

[73] S. Goriparti, E. Miele, F. De Angelis, E. Di Fabrizio, R. Proietti Zaccaria, C. Capiglia, Review on recent progress of nanostructured anode materials for Li-ion batteries, J. Power Sources 257 (2014) 421-443.

[74] K.H. Seng, M.-h. Park, Z.P. Guo, H.K. Liu, J. Cho, Catalytic Role of Ge in Highly Reversible GeO_2/Ge/C Nanocomposite Anode Material for Lithium Batteries, Nano Lett. 13 (2013) 1230-1236.

Accepted manuscript

ACCEPTED MANUSCRIPT

[75] J. Hwang, C. Jo, M.G. Kim, J. Chun, E. Lim, S. Kim, S. Jeong, Y. Kim, J. Lee, Mesoporous Ge/GeO_2/Carbon Lithium-Ion Battery Anodes with High Capacity and High Reversibility, ACS Nano 9 (2015) 5299-5309.

[76] S. Sarkar, R. Borah, A.L. Santhosha, R. Dhanya, C. Narayana, A.J. Bhattacharyya, S.C. Peter, Heterostructure composites of rGO/GeO_2/PANI with enhanced performance for Li ion battery anode material, J. Power Sources 306 (2016) 791-800.

[77] F. Jia, L. Song, W. Wei, P. Qu, M. Xu, Facile one-pot method synthesis CNT-GeO_2 nanocomposite for high performance Li ion battery anode material, New J. Chem. 39 (2015) 689-695.

[78] D.T. Ngo, R.S. Kalubarme, M.G. Chourashiya, C.-N. Park, C.-J. Park, Electrochemical Performance of GeO_2/C Core Shell based Electrodes for Li-ion Batteries, Electrochim. Acta 116 (2014) 203-209.

[79] R. Xu, S. Wu, Y. Du, Z. Zhang, A facile route to dually protected Ge@GeO_2 composites as anode materials for lithium ion battery, Chem. Eng. J. 296 (2016) 349-355.

[80] Q. Yang, T. Sun, J.-Y. Yu, J.-X. Ma, Electrospinning of GeO_2–C fibers and electrochemical application in lithium-ion batteries, Chin. Chem. Lett. 27 (2016) 412-416.

[81] W. Wei, A. Tian, F. Jia, K. Wang, P. Qu, M. Xu, Green synthesis of GeO_2/graphene composites as anode material for lithium-ion batteries with high capacity, RSC Adv. 6 (2016) 87440-87445.

[82] W. He, H. Tian, X. Wang, F. Xin, W. Han, Three-dimensional interconnected network GeO_x/multi-walled CNT composite spheres as high-performance anodes for lithium ion batteries, J. Mater. Chem. A 3 (2015) 19393-19401.

[83] Y. Kim, H. Hwang, K. Lawler, S.W. Martin, J. Cho, Electrochemical behavior of Ge and GeX_2 (X = O, S) glasses: Improved reversibility of the reaction of Li with Ge in a sulfide medium, Electrochim. Acta 53 (2008) 5058-5064.

[84] T. Qiang, J. Fang, Y. Song, Q. Ma, M. Ye, Z. Fang, B. Geng, Ge@C core-shell nanostructures for improved anode rate performance in lithium-ion batteries, RSC Adv. 5 (2015) 17070-17075.

[85] W. Guo, L. Mei, Q. Feng, J. Ma, Facile synthesis of Ge/C nanocomposite as superior battery anode material, Mater. Chem. Phys. 168 (2015) 6-9.

[86] H.-S. Choe, S.-J. Kim, M.-C. Kim, D.-M. Kim, G.-H. Lee, S.-B. Han, D.-H. Kwak, K.-W. Park, Synthesis of Ge/C composites as anodes using glucose as a reductant and carbon source for lithium-ion batteries, RSC Adv. 6 (2016) 72926-72932.

[87] E. Yoo, J. Kim, E. Hosono, H.-s. Zhou, T. Kudo, I. Honma, Large Reversible Li Storage of Graphene Nanosheet Families for Use in Rechargeable Lithium Ion Batteries, Nano Lett. 8 (2008) 2277-2282.

[88] B. Varghese, M.V. Reddy, Z. Yanwu, C.S. Lit, T.C. Hoong, G.V. Subba Rao, B.V.R. Chowdari, A.T.S. Wee, C.T. Lim, C.-H. Sow, Fabrication of NiO Nanowall Electrodes for High Performance Lithium Ion Battery, Chem. Mater. 20 (2008) 3360-3367.

[89] M.V. Reddy, B. Pecquenard, P. Vinatier, A. Levasseur, Cyclic voltammetry and galvanostatic cycling characteristics of $LiNiVO_4$ thin films during lithium insertion and re/de-insertion, Electrochem. Commun. 9 (2007) 409-415.

Accepted manuscript

ACCEPTED MANUSCRIPT

[90] M.-H. Park, K. Kim, J. Kim, J. Cho, Flexible Dimensional Control of High-Capacity Li-Ion-Battery Anodes: From 0D Hollow to 3D Porous Germanium Nanoparticle Assemblies, Adv. Mater. 22 (2010) 415-418.

[91] K.H. Seng, M.-H. Park, Z.P. Guo, H.K. Liu, J. Cho, Self-Assembled Germanium/Carbon Nanostructures as High-Power Anode Material for the Lithium-Ion Battery, Angew. Chem. Int. Ed. 124 (2012) 5755-5759.

[92] X.H. Liu, S. Huang, S.T. Picraux, J. Li, T. Zhu, J.Y. Huang, Reversible Nanopore Formation in Ge Nanowires during Lithiation–Delithiation Cycling: An In Situ Transmission Electron Microscopy Study, Nano Lett. 11 (2011) 3991-3997.

[93] L. Baggetto, P.H.L. Notten, Lithium-Ion (De)Insertion Reaction of Germanium Thin-Film Electrodes: An Electrochemical and In Situ XRD Study, J. Electrochem. Soc. 156 (2009) A169-A175.

[94] L.Y. Lim, S. Fan, H.H. Hng, M.F. Toney, Storage Capacity and Cycling Stability in Ge Anodes: Relationship of Anode Structure and Cycling Rate, Adv. Energy Mater. 5 (2015) 1500599.

[95] S. Yoon, C.-M. Park, H.-J. Sohn, Electrochemical Characterizations of Germanium and Carbon-Coated Germanium Composite Anode for Lithium-Ion Batteries, Electrochem. Solid State Lett. 11 (2008) A42-A45.

ted manuscript

Biographies

David McNulty received his B.Sc in Applied Physics from the University of Limerick in 2009 and his PhD from the Department of Physics in the University of Limerick in 2014. He currently works as a postdoctoral researcher in the Applied Nanoscience Group as part of the School of Chemistry in University College Cork, Ireland. His research is focused on the synthesis, structural and electrochemical characterization of metal oxide and semiconductor

ACCEPTED MANUSCRIPT

nanostructures as anode and cathode materials for next advanced Li-ion batteries. He is an author on more than 20 peer-reviewed articles with more than 200 citations.

Hugh Geaney received a BSc. in Industrial Chemistry and PhD. in Chemistry from the University of Limerick in 2008 and 2012 respectively. His PhD. research focussed on the development of new synthesis methods for Si and Ge nanowires. He then moved to University College Cork as a postdoctoral researcher until 2016, working on Li-O_2 and Li-ion batteries. He has since returned to the University or Limerick as a postdoctoral researcher working on Li-ion full-cells. He is author on more than 50 peer-reviewed articles with in excess of 1200 citations.

Darragh Buckley received his B.Sc. in Chemical Physics from University College Cork in 2014. He is currently working towards his PhD, funded by the Irish Research Council as part of the Applied Nanoscience Group, UCC. His research is focused on solution-processed metal oxide films used in a variety of applications from thin film transistors to optical coating materials by developing the chemical, structural, optical and electrical phenomena.

Colm O'Dwyer received his B.Sc. in applied physics (1999) and Ph.D. in physics (2003) from the University of Limerick. After postdoctoral research in nanolithography using magneto-optically-trapped, ultracold Cs atoms beams at the University of Toulouse III in France, he developed inorganic nanostructures at Tyndall National Institute. He was a Science Foundation Ireland Stokes Lecturer at the University of Limerick. At University College Cork, he leads the Applied Nanoscience Group. He is Chair of the Electronics & Photonics Division of ECS, and organized >25 symposia in nanoscience, solid-state science and semiconductor electrochemistry. He is a Fellow of the Institute of Physics.

Accepted manuscript

ACCEPTED MANUSCRIPT

Highlights

- Crystalline macroporous GeO_2 inverse opals exhibit state-of-the-art capacity retention, voltage stability and a very long cycle life.
- The anode uses structured porosity to remove the need for conductive additives or binders to form a slurry or electrode casting.
- Detailed insight in to the mechanism of reversibly lithiation of Ge from interconnected GeO_2 nanocrystals.
- Exceptional voltage stability and rate performance, with high capacity up to 1 A/g rates.
- Relatively low temperature route to Ge-based nanomaterials for high capacity Li-ion battery anodes.

Accepted manuscript

Graphical abstract

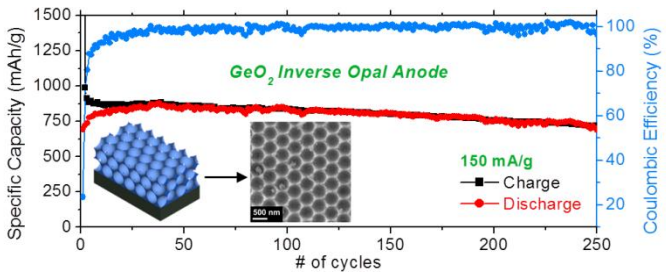

Accepted manuscript